Analytical piecewise radial distortion model for precision camera calibration

L. Ma, Y.Q. Chen and K.L. Moore

Abstract: The common approach to radial distortion is by the means of polynomial approximation, which introduces distortion-specific parameters into the camera model and requires estimation of these distortion parameters. The task of estimating radial distortion is to find a radial distortion model that allows easy undistortion as well as satisfactory accuracy. This article presents a new piecewise radial distortion model with easy analytical undistortion formula. The motivation for seeking a piecewise radial distortion model is that, when a camera is resulted in a low quality during manufacturing, the nonlinear radial distortion can be complex. Using low order polynomials to approximate the radial distortion might not be precise enough. In contrast, higher order polynomials suffer from the inverse problem. With the new piecewise radial distortion function, more flexibility is obtained and the radial undistortion can be performed analytically. Experimental results are presented to show that with this new piecewise radial distortion model, better performance can be achieved than using the single function. Further, a comparable performance with the conventional polynomial model using two coefficients can also be accomplished.

1 Introduction

Cameras are widely used in many engineering automation processes from visual monitoring and visual metrology to real-time visual servoing or visual following. We will focus on a new camera distortion model that uses a piecewise radial distortion function yet having an analytical undistortion formula, that is, no numerical iteration is required for undistortion.

Camera calibration is to estimate a set of parameters that describes the camera's imaging process. Assuming that radial distortion occurs along the radial direction from the centre of distortion (which is further assumed to be the same as the principal point), the imaging process can be illustrated by

$$\underbrace{\begin{bmatrix} u \\ v \\ 1 \end{bmatrix} = \begin{bmatrix} \alpha & \gamma & u_0 \\ 0 & \beta & v_0 \\ 0 & 0 & 1 \end{bmatrix}}_{A} \begin{bmatrix} x \\ y \\ 1 \end{bmatrix} \longrightarrow \begin{cases} u_d - u_0 = (u - u_0) f(r) \\ v_d - v_0 = (v - v_0) f(r) \end{cases}$$

Camera frame to image plane (in pixels) | Distortion in the image plane

or

$$\begin{cases} x_d = x f(r) \\ y_d = y f(r) \end{cases} \longrightarrow \underbrace{\begin{bmatrix} u_d \\ v_d \\ 1 \end{bmatrix} = \begin{bmatrix} \alpha & \gamma & u_0 \\ 0 & \beta & v_0 \\ 0 & 0 & 1 \end{bmatrix}}_{A} \begin{bmatrix} x_d \\ y_d \\ 1 \end{bmatrix}$$

Distortion in the camera frame | Camera frame to image plane (in pixels)

where $x = X^c/Z^c$, $y = Y^c/Z^c$ and $[X^c, Y^c, Z^c]^T$ denotes a point in the camera frame; matrix A fully depends on the camera's five intrinsic parameters (α, γ, β, u_0, v_0), with (α, β) being two scalars in the two image axes, (u_0, v_0) the coordinates of the principal point and γ describing the skewness of the two image axes; (u, v) and (u_d, v_d) are the distortion-free and distorted image points on the image plane, respectively; (x, y) and (x_d, y_d) are the distortion-free and distorted points in the camera frame, respectively; function $f(r)$ models the radial distortion that is in terms of radius r only with $r = \sqrt{(x^2 + y^2)}$.

Virtually, all imaging devices introduce certain amount of nonlinear distortions, among which the radial distortion is the most severe part [1, 2]. The removal or alleviation of the radial distortion is commonly performed by first applying a parametric radial distortion model, estimating the distortion coefficients and then correcting the distortion. The radial distortion is suggested to be governed by the following polynomial equation [3–6]

$$r_d = r f(r) = r(1 + k_1 r^2 + k_2 r^4 + k_3 r^6 + \cdots) \qquad (1)$$

where k_1, k_2, k_3, ... are the distortion coefficients. When using two coefficients, the relationship between the

IEE Proceedings online no. 20045035

doi:10.1049/ip-vis:20045035

Paper first received 25th May 2004 and in final revised form 3rd January 2006

L. Ma is with the Department of Aerospace and Ocean Engineering, Virginia Tech, 215 Randolph Hall, Blacksburg, VA, 24061, USA

Y.Q. Chen is with the Department of Electrical and Computer Engineering, Utah State University, 4160 Old Main Hill, Logan, UT, 84322, USA

K.L. Moore is with the Division of Engineering, Colorado School of Mines, Brown Building 305, 1610 Illinois Street, Golden, CO, 80401, USA

E-mail: lma05@vt.edu

distorted and the undistorted radial distances becomes [3]

$$r_d = r(1 + k_1 r^2 + k_2 r^4) \tag{2}$$

Until recently, the most commonly used radial distortion model had been in the polynomial form of (2), although other models, such as the division model [7] and the fish-eye radial distortion models (the fish-eye transform [1] and the field-of-view [8]), are available in the literature. The inverse of the polynomial function in (2) is difficult to perform analytically. Modelling the radial distortion precisely with an analytical inverse function is the focus of this article.

The relationship between r_d and r can also be modelled as [9]

$$r_d = rf(r) = r(1 + k_1 r + k_2 r^2 + k_3 r^3 + \cdots) \tag{3}$$

To overcome the inversion problem, the above model with two coefficients is studied in the works of Ma *et al.* [10, p. 3, 11], which is

$$f(r) = 1 + k_1 r + k_2 r^2 \tag{4}$$

whose appealing feature lies in its satisfactory accuracy as well as in the the existence of an easy analytical undistortion formula [11]. The polynomial radial distortion model in (4), together with the commonly used model (2), acts as the benchmark for evaluating the performance of the piecewise radial distortion model proposed in Section 2.

Among the camera calibration algorithms, a planar-based calibration method described in the work of Zhang [3] is used in this article, in which detailed procedures can be summarised as: (i) estimation of intrinsic parameters; (ii) estimation of extrinsic parameters; (iii) estimation of distortion coefficients and (iv) full-scale nonlinear optimisation. In the full-scale nonlinear optimisation, the following objective function J [3]

$$J = \sum_{i=1}^{N_{im}} \sum_{j=1}^{n} \|m_{ij} - \hat{m}(\boldsymbol{A}, k, R_i, t_i, M_j)\|^2 \tag{5}$$

is used, where M_j is the jth 3D point in the world frame with $Z^w = 0$; $\hat{m}$ $(\boldsymbol{A}, k, R_i, t_i, M_j)$ is the projection of point M_j in the ith image using the estimated parameters; k denotes the distortion coefficients; n is the number of feature points in the coplanar calibration object and N_{im} is the number of images taken for calibration [3, 11].

2 Piecewise radial distortion model

A two-segment radial distortion function is proposed and illustrated in Fig. 1, in which each segment is a function

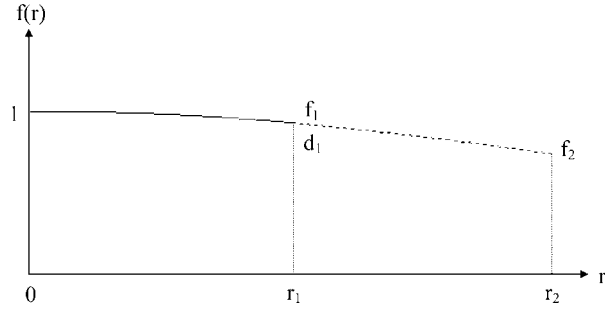

Fig. 1 *Smooth piecewise function (two-segment)*

of the form

$$\begin{aligned} f_1(r) &= a_0 + a_1 r + a_2 r^2, \quad \text{for } r \in [0, r_1] \\ f_2(r) &= b_0 + b_1 r + b_2 r^2, \quad \text{for } r \in (r_1, r_2] \end{aligned} \tag{6}$$

with $r_1 = r_2/2$. Each segment in (6) is motivated from the polynomial function (4) that has been studied in the work of Ma *et al.* [10, p. 3]. We are interested in estimating the coefficients (a_0, a_1, a_2) and (b_0, b_1, b_2) such that the two polynomials are continuous and smooth at the interior knot $r = r_1$. The reason for choosing a distortion function in (4) for each segment is that the radial undistortion can be performed using the analytical procedures described in Ma *et al.* [11] with no iterations.

To ensure that the overall function (6) is continuous and smooth across the interior knot (Besides the requirement of continuity and smoothness at the interior knot r_1, the estimated $f(r)$ curve has to be monotonous to ensure the uniqueness in the $r_d \leftrightarrow r$ relationship in the context of lens distortion modelling. However, this additional constraint is not necessary because it is inherent in the physical lens to be modelled.), the following six constraints can be applied

$$\begin{aligned} f_1(0) &= 1 \\ a_0 + a_1 r_1 + a_2 r_1^2 &= f_1 \\ a_1 + 2a_2 r_1 &= d_1 \\ b_0 + b_1 r_1 + b_2 r_1^2 &= f_1 \\ b_1 + 2b_2 r_1 &= d_1 \\ b_0 + b_1 r_2 + b_2 r_2^2 &= f_2 \end{aligned} \tag{7}$$

where $f_1 = f_1(r_1) = f_2(r_1)$, $f_2 = f_2(r_2)$ and $d_1 = \dot{f}_1(r_1) = \dot{f}_2(r_1)$. By enforcing that the two segments have the same value and derivative at the interior knot r_1, the resultant single function is guaranteed to be continuous and smooth over the whole range $[0, r_2]$. As each interior knot provides four constraints to make the resultant single function smooth, in order to estimate the coefficients (a_0, a_1, a_2) and (b_0, b_1, b_2) uniquely, we need another two constraints, which are chosen to be $f_1(0)$ and $f_2(r_2)$ in (7).

As the coefficients (a_0, a_1, a_2) and (b_0, b_1, b_2) in (7) can be calculated uniquely from (f_1, d_1, f_2) by

$$\begin{aligned} a_0 &= 1 \\ a_1 &= \frac{(-2 - r_1 d_1 + 2f_1)}{r_1} \\ a_2 &= \frac{(1 + r_1 d_1 - f_1)}{r_1^2} \\ b_2 &= \frac{(f_2 - f_1 + r_1 d_1 - r_2 d_1)}{(r_1 - r_2)^2} \\ b_1 &= d_1 - 2b_2 r_1 \\ b_0 &= f_1 - d_1 r_1 + b_2 r_1^2 \end{aligned} \tag{8}$$

the radial distortion coefficients that are used in the nonlinear optimisation for the piecewise radial distortion model can be chosen to be (f_1, d_1, f_2) with the initial values (1, 0, 1), which has only one extra coefficient compared with the single model (4). During the nonlinear optimisation process, the coefficients (a_0, a_1, a_2) and (b_0, b_1, b_2) are calculated from (8) in each iteration.

The purpose of this work is to show that the proposed piecewise radial distortion model achieves:

1. Given r_d and the distortion coefficients, the solution of r from r_d has closed-form solution.
2. It approximates the commonly used distortion model (2) with higher accuracy than the single function (4).

3 Experimental results and validations

A series of experiments are performed in this section to validate the proposed piecewise radial distortion model. First, using the three distortion models (2), (4) and (6), the final values of the objective function J of three groups of testing images are given in Section 3.1. The model selection problem among the three models is further discussed using geometric akaike information criterion (AIC) and geometric minimum description length (MDL) criteria [12, 13] in Section 3.2. Then, we simulate the whole imaging process by constructing a virtual camera with known camera parameters and distortion model in Section 3.3. We generate images with the noise of a planar calibration target. Secondly, we test whether the distortion coefficients are accurately estimated by the idea 'straight lines have to be straight'. Simulation is further presented in Section 3.4 to show how a more accurately modelled radial distortion affects the application of computer vision in vision-based feedback control, in which the seemingly insignificant advantage of a more accurate distortion model manifests noticeable difference in the control performance.

3.1 Initial model comparison

In this section, comparisons are made among the two-segment piecewise distortion model (6), the single model (4) and the commonly used model (2) on the basis of final value of the objective function J in (5) after nonlinear optimisation by the Matlab function `fminunc`, as common approach to camera calibration is to perform a full-scale nonlinear optimisation for all parameters. Using the public domain-testing images of dimension 640×480 [14], the desktop camera images (320×240) (a colour camera in our Center for Self-Organizing and Intellegent Systems, CSOIS) and the omindirectional inspection system (ODIS) camera images (320×240) [11] (the camera on ODIS robot built in our CSOIS), the final values of J, the estimated distortion coefficients and the five estimated intrinsic parameters (α, β, γ, u_0, v_0) are summarised in Table 1 in which the listed distortion coefficients are (k_1, k_2) for the single models (2) and (4) and (f_1, d_1, f_2) for the piecewise. The extracted corners for the model plane of the desktop and the ODIS cameras have been presented in Ma *et al.* [11].

From Table 1, it can be observed that the values of J using the piecewise model for the three groups of testing images are always less than those using the single function (4). Further, the fitting residuals are closer to those of model (2). For the ODIS images, the value of J of the piecewise model is even smaller than that of model (2). The comparison between model (6) with models (2) and (4) might not be fair because the new piecewise model has one more coefficient. Hence, more simulations and discussions are presented in Sections 3.2 and 3.3 for the validation of the proposed piecewise model regarding its accuracy improvement and stability. Our main point is to emphasise that by applying the piecewise idea, higher accuracy can be achieved without sacrificing the property of having analytical undistortion function.

In performing the comparisons of the distortion models using the three groups of test images, we first use the calibration procedures described in Zhang [3] to calibrate the camera's intrinsic and extrinsic parameters, which serve as the initial guesses in the nonlinear optimisation step. By using (1, 0, 1) as the initial guess for (f_1, d_1, f_2), the whole set of camera parameters are determined after performing a full-scale nonlinear optimisation.

One issue in the implementation of the nonlinear optimisation is how to decide r_2, which is related to the estimated extrinsic parameters that are changing from iteration to iteration during the nonlinear optimisation process. In our implementation, for each camera, five images are taken where there are 64×4 feature points on each image. r_2 is chosen to be the maximum r of all the extracted feature points on the five images for each iteration.

3.2 Distortion model selection

Classical criteria that are used in the computer vision to assess the accuracy of calibration include the radial distortion as one part inherently [15]. However, the idea to choose among candidate models the one that gives the smallest residual does not work, because a model with more degrees of freedom (DOFs) might always be chosen, as it is more likely to yield a smaller residual. To compare the distortion models fairly, the over-fit caused by more DOFs in the distortion model needs to be compensated. Hence, a comparison that is solely based on the fitting residual of the full-scale nonlinear optimisation (5), as performed in Section 3.1, is not enough [11].

Model selection is one of the central subjects of statistical inference. In Kanatani [12], two widely adopted criteria for statistical model selection, Akaike's AIC and Rissanen's MDL, have been generalised as GAIC and GMDL for the geometric fitting such that the GAIC and GMDL criteria can be helpful for geometric problems considered in the computer vision. The GAIC and GMDL of a model S are

Table 1: Comparison of radial distortion models using three groups of testing images

Images	Model	J	Distortion coefficients			Intrinsic parameters (α, γ, u_0, β, v_0)				
Public	(2)	144.8802	−0.2286	0.1905	–	832.4860	0.2042	303.9605	832.5157	206.5811
	(4)	145.6592	−0.0215	−0.1566	–	833.6508	0.2075	303.9847	833.6866	206.5553
	(6)	144.8874	0.9908	−0.0936	0.9653	831.7068	0.2047	303.9738	831.7362	206.5670
Desktop	(2)	778.9767	−0.3435	0.1232	–	277.1449	−0.5731	153.9882	270.5582	119.8105
	(4)	803.3074	−0.1067	−0.1577	–	282.5642	−0.6199	154.4913	275.9019	120.0924
	(6)	782.5865	0.9387	−0.2695	0.8066	277.4852	−0.5757	154.0058	270.9052	119.7416
ODIS	(2)	840.2650	−0.3554	0.1633	–	260.7658	−0.2741	140.0581	255.1489	113.1727
	(4)	851.2619	−0.1192	−0.1365	–	266.0850	−0.3677	139.9198	260.3133	113.2412
	(6)	838.5678	0.9410	−0.2563	0.8270	261.9485	−0.2875	140.2521	256.3134	113.0856

Table 2: Model selection using GAIC and GMDL

Images	Criterion	(2)	(4)	(6)
Public	GAIC (10^3)	0.4355	0.4363	0.4357
	GMDL (10^3)	2.3394	2.3402	2.3411
Desktop	GAIC (10^3)	2.3418	2.3661	2.3466
	GMDL (10^4)	1.0181	1.0205	1.0192
ODIS	GAIC (10^3)	2.5261	2.5371	2.5257
	GMDL (10^4)	1.0918	1.0929	1.0924

defined as [12, pp. 4, 7; 13, p. 4]

$$\mathrm{GAIC}(S) = J(S) + 2(dN + p)\varepsilon^2 \tag{9}$$

and

$$\mathrm{GMDL}(S) = J(S) - (dN + p)\varepsilon^2 \log\left(\frac{\varepsilon}{L}\right)^2 \tag{10}$$

where $J(S)$ is the fitting residual when data of size N are fitted to the model S. p is the DOF of the model S. $d = m - d_c$, with m the dimension of the observed data and d_c the co-dimension of the model. L is a reference length, which is taken as the image width in El-Melegy and Farag [13, p. 5]. ε is the noise level in the data set.

In the context of lens distortion modelling, in order to apply the GAIC and GMDL, the noise level ε needs to be known. An unbiased estimate of ε can be obtained from the most commonly used candidate model (2), denoted by S^0, as [12, p. 8; 13, p. 5]

$$\hat{\varepsilon}^2 = \frac{J(S^0)}{d_c N - p^0} \tag{11}$$

where p^0 is the DOF of model S^0. In this experiment, both the GAIC and GMDL are applied to validate the proposed model relevance, and the results are shown in Table 2.

An observation from Table 2 shows that the lens model selection generally favours model (6) better than (4), with one exception, when using the GMDL for the public images, where model (4) will be selected instead of (6). In this case, a possible explanation is that the advantage gained by the piecewise idea is not significant enough to compensate the over-fitting because of the extra one DOF in the model. It is also noticed that when using the GAIC for the ODIS images, model (6) is even better than the commonly used model (2). From these observations, it can be concluded that the proposed piecewise model can achieve higher accuracy than the single function (4) and even comparable accuracy against the commonly used model (2), especially when the distortion becomes more severe.

3.3 Straight lines have to be straight

The GAIC- and GMDL-based model selection, as presented in Section 3.2, uses the fitting residual after the nonlinear optimisation process, with the extra DOF in the distortion model being compensated. In this section, we imagine the measurements that only involve the distortion on the basis of the idea that if the distortion coefficients are accurately estimated, straight lines will remain straight. As the true values of the intrinsic parameters and the distortion coefficients are by no means exactly known from manufactured cameras as used in Sections 3.1 and 3.2, we construct a virtual camera via simulation to test whether the undistorted straight lines remain straight.

When constructing the virtual camera, we assume that the camera has the following parameters

$$\text{Intrinsic matrix } \boldsymbol{A} = \begin{bmatrix} 200 & 0.5 & 110 \\ 0 & 200 & 110 \\ 0 & 0 & 1 \end{bmatrix} \tag{12}$$

$$\text{Distortion coefficients } k = (k_1, k_2) = (-0.22, 0.19)$$

$$\text{Distortion model } f(r) = 1 + k_1 r^2 + k_2 r^4$$

To simulate the whole imaging and calibration process, the extrinsic parameters of the camera during calibration are taken as

$$\mathbf{RT} = \begin{bmatrix} -0.1 & 0.1 & 0.2 & -10 & -10 & 25 \\ 0.2 & 0.5236 & 0.1 & -10 & -10 & 28 \\ 0.1 & -0.3927 & 0.01 & -10 & -10 & 28 \\ 0.4488 & 0.3142 & -0.21 & -10 & -10 & 30 \\ -0.2094 & 0.1 & 0.1 & -10 & -10 & 28 \end{bmatrix} \tag{13}$$

where each row denotes the transformation between the camera and the world coordinate system and the first three elements in each row denote the ZYZ Euler angles $(\theta_a, \theta_b, \theta_c)$ [11]. The remaining three elements denote the translational vector. The above choice of the camera parameters, including the intrinsic parameters, extrinsic parameters and the distortion coefficients, is without any preference. The distortion model selected in the form of (2) is because of its common usage and acceptance.

The simulated calibration process is performed eight times and the calibration results, using the three different distortion models, are shown in Tables 3, 4 and 5, respectively, where the first to the eighth columns in the three

Table 3: Variation of the calibration results using the distortion model (2)

	Trial								Mean	STD
	1	2	3	4	5	6	7	8		
α	202.9645	200.3229	199.9081	200.6867	200.3113	200.4332	200.0304	201.3989	200.7570	1.0022
γ	0.5664	0.3196	0.3671	0.5393	0.3231	0.4299	0.5158	0.5693	0.4538	0.1072
u_0	110.6417	109.1198	111.9734	109.9408	110.3896	110.3842	109.2275	108.2256	109.9878	1.1419
β	202.6473	200.5361	199.5521	200.8055	200.2543	200.2972	199.9590	201.5035	200.6944	0.9786
v_0	110.1448	108.9201	109.4174	110.0071	108.7463	109.3735	110.8114	110.7411	109.7702	0.7816
k_1	−0.2400	−0.2243	−0.2277	−0.2116	−0.2050	−0.2301	−0.2189	−0.2231	−0.2226	0.0109
k_2	0.2465	0.1896	0.2072	0.1612	0.1490	0.2072	0.1917	0.1924	0.1931	0.0298
RMS	0.8030	0.8170	0.8320	0.8062	0.8230	0.8301	0.8090	0.8158	0.8170	0.0108

Distortion coefficients (k_1, k_2) in the first column refer to model (2).

Table 4: Variation of the calibration results using the distortion model (4)

	Trial								Mean	STD
	1	2	3	4	5	6	7	8		
α	205.4840	202.2318	201.6399	201.9833	201.5445	202.3588	202.0539	202.9823	202.5348	1.2727
γ	0.5585	0.3276	0.3669	0.5500	0.3235	0.4313	0.5126	0.5786	0.4561	0.1070
u_0	110.4079	108.9229	111.6551	109.9089	110.1017	109.7364	108.7734	107.8958	109.6753	1.1491
β	205.1939	202.4805	201.3216	202.1274	201.5213	202.2779	202.0213	203.1322	202.5095	1.2201
v_0	109.7839	108.8650	109.2199	109.9854	108.6129	109.2036	110.5840	110.6764	109.6164	0.7675
k_1	−0.1129	−0.0913	−0.0893	−0.0703	−0.0647	−0.0910	−0.0892	−0.0811	−0.0862	0.0147
k_2	−0.0028	−0.0347	−0.0341	−0.0603	−0.0650	−0.0342	−0.0320	−0.0464	−0.0387	0.0193
RMS	0.8031	0.8173	0.8344	0.8072	0.8242	0.8320	0.8093	0.8172	0.8181	0.0114

Distortion coefficients (k_1, k_2) in the first column refer to model (4).

tables display the calibration results of each trial. The last row in each table, indicated by RMS, displays the root of mean squared distances, in pixels, between the detected image points and the projected ones. In each calibration, five images of the calibration target are generated and corrupted with the noise of normal distribution with zero mean and standard deviation $1/2$. It can be observed that the sample derivations for all the parameters in the three tables are quite small, showing that the applied calibration procedure with the distortion models in comparison is stable.

So far, we have demonstrated the model relevance of the proposed piecewise model via the simulated virtual camera, using the RMS representation in Tables 3, 4 and 5. Next, we want to evaluate the accuracy of the calibrated distortion only. One way to evaluate the accuracy of the distortion is to examine the resultant $f(r) \leftrightarrow r$ curves. Though the calibrated distortion coefficients associated with certain model are achieved through the full-scale nonlinear optimisation, a more accurate calibration should guarantee the more closeness of the estimated distortions to its true values. Another way to look at the distortion calibration accuracy is to test whether straight lines, that have been distorted by a 'true' model can be undistorted back properly using the calibrated camera parameters, that is, whether straight lines that have gone through the distortion–undistortion process remain straight.

The resultant $f(r) \leftrightarrow r$ curves when using the three models are presented in Fig. 2. The corresponding undistorted straight lines are shown in Fig. 3. In Fig. 3, red is used for the true camera parameters assumed in (12), green for the calibrated camera parameters using distortion model (4) and blue for (6). From Fig. 2, it can be observed that the estimated $f(r) \leftrightarrow r$ curves when using the piecewise model are closer to their true values than when using the single model (4). Fig. 3 manifests a similar observation in which the undistorted green lines using model (4) deviate from their true positions much more significantly. In Fig. 3, because of this effect, the plotted red, green, and blue lines coincide with each other around the centre of distortion. As the radius increases, lines of different colours begin to separate and their difference become noticeable.

The experimental results presented so far in Section 3.3 only validate the model relevance of the proposed piecewise distortion model. That is, the camera calibration procedure adopting the piecewise model remains stable, as can be seen from Tables 3, 4 and 5, and straight lines remain almost straight, as shown in Figs. 2 and 3. From this fact, no conclusion can be drawn regarding the 'model selection' or 'model comparison' because of the extra DOF in the piecewise model. Actually, whether a certain distortion model best represents a lens distortion is indeed camera dependent. Calculations of the GAIC and GMDL criteria of the virtual camera as constructed in (12) and (13) do not show an improvement of model (6) over (4). However, when constructing a different virtual camera, using the following parameters

$$\boldsymbol{A} = \begin{bmatrix} 260 & -0.2741 & 140.0581 \\ 0 & 255.1489 & 113.1727 \\ 0 & 0 & 1 \end{bmatrix}$$
$$k = (k_1, k_2) = (-0.3554, 0.1633) \qquad (14)$$
$$f(r) = 1 + k_1 r^2 + k_2 r^4$$

Table 5: Variation of the calibration results using the piecewise distortion model (6)

	Trial								Mean	STD
	1	2	3	4	5	6	7	8		
α	204.1263	201.3673	199.1406	200.8552	199.7450	200.1523	200.8830	201.4722	200.9678	1.5075
γ	0.5654	0.3285	0.3690	0.5465	0.3305	0.4272	0.5167	0.5722	0.4570	0.1054
u_0	110.6482	108.9809	111.9612	109.8845	110.3877	110.3090	109.0915	108.1452	109.9260	1.1824
β	203.8152	201.6002	198.7878	200.9840	199.6890	200.0209	200.8246	201.5868	200.9136	1.5200
v_0	109.9494	108.9224	109.3269	110.0051	108.7831	109.2170	110.6859	110.6630	109.6941	0.7437
f_1	0.9679	0.9687	0.9783	0.9751	0.9793	0.9757	0.9712	0.9750	0.9739	0.0042
d_1	−0.1279	−0.1251	−0.1383	−0.1244	−0.1291	−0.1370	−0.1227	−0.1289	−0.1292	0.0057
f_2	0.9304	0.9254	0.9384	0.9309	0.9357	0.9347	0.9305	0.9330	0.9324	0.0040
RMS	0.8025	0.8170	0.8321	0.8067	0.8229	0.8303	0.8088	0.8163	0.8171	0.0108

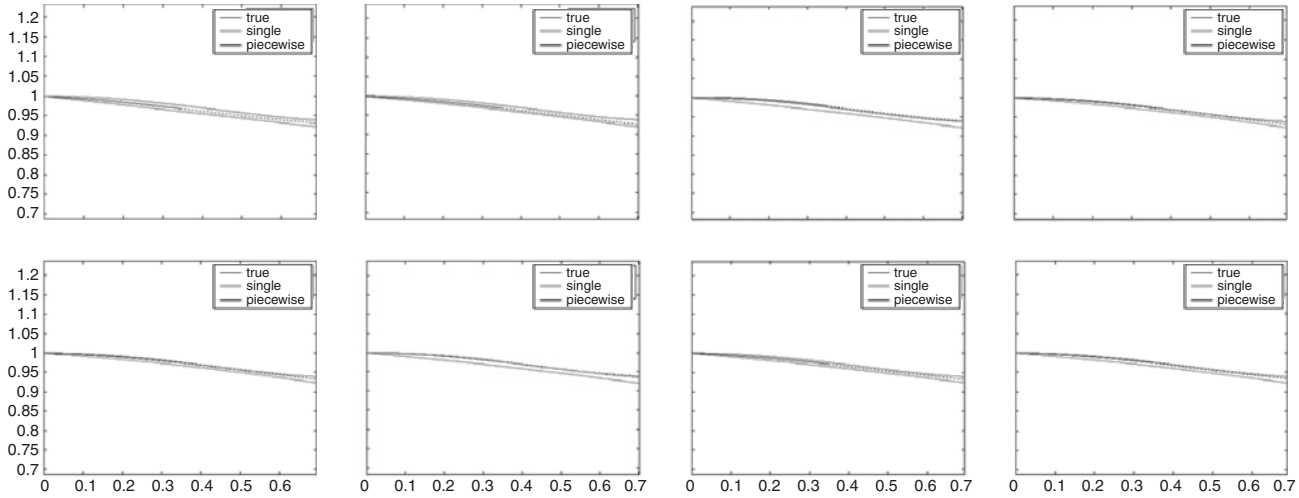

Fig. 2 *f(r) ↔ r relationship when using the three distortion models (simulated camera)*

and

$$\mathbf{RT} = \begin{bmatrix} -1.89 & 2.83 & -1.95 & 12.16 & -12.64 & -31.90 \\ -1.26 & 2.94 & -1.29 & 10.39 & -16.31 & -33.44 \\ -1.51 & 2.78 & -1.53 & 13.03 & -12.09 & -24.50 \\ -1.46 & 2.81 & -1.47 & 12.88 & -13.07 & -27.26 \\ -0.80 & 2.59 & -0.74 & 11.16 & -11.69 & -23.99 \end{bmatrix} \tag{15}$$

which is close to the ODIS camera as shown in Table 1, an improvement of model (6) over (4) is apparent, which is shown in Table 6.

3.4 Simulation of application in vision feedback control

In Sections 3.2 and 3.3, we have validated the proposed piecewise radial distortion model via both qualitative and quantitative criteria using both simulated virtual camera and real manufactured cameras. In this section, we shall briefly show, via one example, how the improvement in the lens distortion modelling can be noticeable in vision-based feedback control, which can be a real application of the computer vision.

Consider a stationary camera observing a moving object whose motion is governed by the following affine motion

$$\begin{bmatrix} \dot{X}(t) \\ \dot{Y}(t) \\ \dot{Z}(t) \end{bmatrix} = \begin{bmatrix} a_{11} & a_{12} & a_{13} \\ a_{21} & a_{22} & a_{23} \\ a_{31} & a_{32} & a_{33} \end{bmatrix} \begin{bmatrix} X(t) \\ Y(t) \\ Z(t) \end{bmatrix} + \begin{bmatrix} b_1 \\ b_2 \\ b_3 \end{bmatrix} \tag{16}$$

One problem, generally referred to as the range identification problem of a perspective dynamic system, is to estimate the depth of such an object, denoted by $y_3(t) = 1/Z(t)$, with an unknown initial condition from observations on the image plane, where the motion parameters $a_{i,j}$ and b_i in (16) for $i, j = 1, 2, 3$ are assumed to be known [16, 17, p. 1]. In a range identification problem, it is always assumed that the following information can be derived from the observations on the image plane

$$y_1(t) = \frac{X(t)}{Z(t)}, \quad y_2(t) = \frac{Y(t)}{Z(t)} \tag{17}$$

That is, the observed feature points on the image plane have been undistorted and transformed to the camera frame at $Z^c = 1$, where the focal length is assumed to be 1 without loss of generality.

The range identification problem can be solved via nonlinear observers for the linear system (16) with the homogeneous output (17). In Fig. 4, the observer performance is presented by applying the observer proposed in Jankovic and Ghosh [16] with the same observer parameters

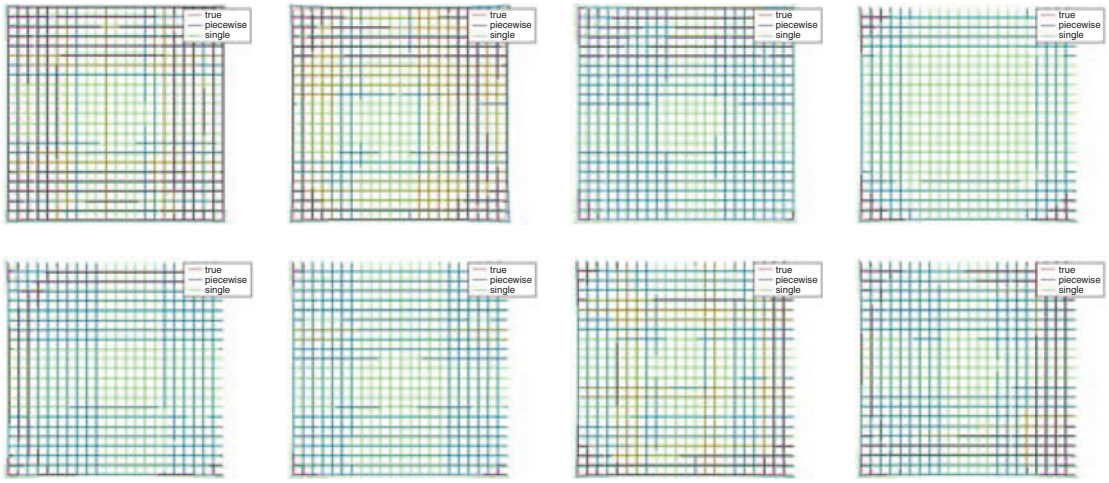

Fig. 3 *Undistorted lines when using the three distortion models (simulated camera)*

Table 6: Model comparison of the simulated camera in (14) and (15)

Trial	Criterion	(2)	(4)	(6)
1	GAIC	1.1055	1.1137	1.1065
	GMDL	5.0830	5.0912	5.0871
2	GAIC	1.1551	1.1609	1.1567
	GMDL	5.2942	5.3000	5.2990
3	GAIC	1.1209	1.1309	1.1224
	GMDL	5.1485	5.1585	5.1532
4	GAIC	1.0630	1.0678	1.0648
	GMDL	4.9016	4.9064	4.9063
5	GAIC	1.1598	1.1638	1.1611
	GMDL	5.3142	5.3182	5.3188
6	GAIC	1.1143	1.1231	1.1155
	GMDL	5.1202	5.1291	5.1246
7	GAIC	1.1089	1.1162	1.1101
	GMDL	5.0973	5.1047	5.1017
8	GAIC	1.0801	1.0868	1.0810
	GMDL	4.9745	4.9812	4.9785
Mean	GAIC	1.1135	1.1204	1.1148
	GMDL	5.1167	5.1237	5.1211

Noise of zero mean and standard deviation 1/4 is added to the extracted features on the image plane when constructing the virtual camera in (14) and (15).

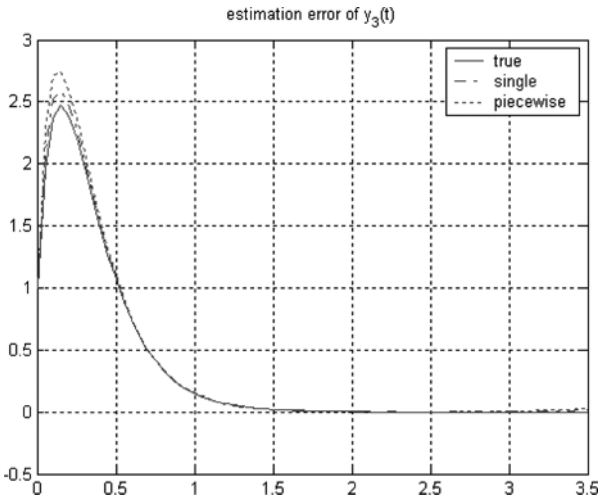

Fig. 4 *Observer performance under the effect of radial undistortion*

for the simulated virtual camera in (12) and (13) under the cases of: (i) ideal situation with no distortion; (ii) undistorted information using model (4) and (iii) undistorted information using (6). (As this paper is mainly concerned with the radial distortion modelling, parameters of the nonlinear observer are not presented. The reader is referred to the work of Ma *et al.* [17, p. 5] for the detailed observer information.) It can be observed that application of the piecewise model helps to reduce the observer overshoot. This phenomenon has been observed throughout our calibration of the virtual cameras.

4 Concluding remarks

This article proposes a new piecewise polynomial radial distortion model for camera calibration. The appealing part of this piecewise model is that it preserves high accuracy and the property of having analytical undistortion formula for each segment. Experimental results are presented to show that this new piecewise radial distortion model can be quite accurate and performance improvement is achieved compared with the corresponding single radial distortion function. Further, a comparable performance with the conventional polynomial radial distortion model using two coefficients can also be accomplished.

5 References

1 Devernay, F., and Faugeras, O.: 'Straight lines have to be straight', *Mach. Vis. Appl.*, 2001, **13**, (1), pp. 14–24
2 Tsai, R.Y.: 'A versatile camera calibration technique for high-accuracy 3D machine vision metrology using off-the-shelf TV cameras and lenses', *IEEE J. Robot. Autom.*, 1987, **3**, (4), pp. 323–344
3 Zhang, Z.: 'Flexible camera calibration by viewing a plane from unknown orientation'. IEEE Int. Conf. on Computer Vision, September 1999, pp. 666–673
4 Slama, C.C.: 'Manual of photogrammetry' (American Society of Photogrammetry, Falls Church, 1980, 4th edn).
5 Heikkila, J., and Silven, O.: 'A four-step camera calibration procedure with implicit image correction'. IEEE Computer Society Conf. on Computer Vision and Pattern Recognition, San Juan, Puerto Rico, 1997, pp. 1106–1112
6 Heikkila, J., and Silven, O.: 'Calibration procedure for short focal length off-the-shelf CCD cameras'. Proc. 13th Int. Conf. on Pattern Recognition, Vienna, Austria, 1996, pp. 166–170
7 Fitzgibbon, A.W.: 'Simultaneous linear estimation of multiple view geometry and lens distortion'. Proc. Conf. on Computer Vision and Pattern Recognition, Kauai, Hawaii, 2001, pp. 125–132
8 Basu, A., and Licardie, S.: 'Alternative models for fish-eye lenses', *Pattern Recognit. Lett.*, 1995, **16**, (4), pp. 433–441
9 Hartley, R., and Zisserman, A.: 'Multiple view geometry' (Cambridge University Press, Cambridge, UK, 2000, 2nd edn.)
10 Ma, L., Chen, Y.Q., and Moore, K.L.: 'Flexible camera calibration using a new analytical radial undistortion formula with application to mobile robot localization'. IEEE Int. Symp. on Intelligent Control, Houston, October 2003
11 Ma, L., Chen, Y.Q., and Moore, K.L.: 'Rational radial distortion models of camera lenses with analytical solution for distortion correction', *Int. J. Inf. Acquis.*, 2004, **1**, (2), pp. 135–147
12 Kanatani, K.: 'Model selection for geometric inference'. 5th Asian Conf. on Computer Vision, January 2002
13 El-Melegy, M.T., and Farag, A.A.: 'Nonmetric lens distortion calibration: closed-form solutions, robust estimation and model selection'. IEEE Int. Conf. on Computer Vision, Nice, France, 2003
14 Zhang, Z.: 'Experimental data and result for camera calibration', Microsoft Research Technical Report, 1998, http://research.microsoft.com/~zhang/calib/
15 Weng, J., Cohen, P., and Herniou, M.: 'Camera calibration with distortion models and accuracy evaluation', *IEEE Trans. Pattern Anal. Mach. Intell.*, 1992, **14**, (10), pp. 965–980
16 Jankovic, M., and Ghosh, B.K.: 'Visually guided ranging from observations of points, lines and curves via an identifier based nonlinear observer', *Syst. Control Lett.*, 1995, **25**, pp. 63–73
17 Ma, L., Chen, Y.Q., and Moore, K.L.: 'Range identification for perspective dynamic systems using linear approximation'. IEEE Int. Conf. Robotics and Automation, New Orleans, 26 April–1 May 2004, pp. 1658–1663